Proposal to the Q-PAC at RCNP for the LEPS detector

K^{*0} and Λ photoproduction using linearly polarized photons

Spokesmen: Prof. K. Hicks[1] and Prof. K. Joo[2]
[1] *Ohio University, Athens, Ohio 45701 USA*
[2] *University of Connecticut, Storrs, CT 06269 USA*
emails: hicks@ohio.edu and kjoo@phys.uconn.edu

Collaborators:
T. Nakano, M. Sumihama, T. Mibe, M. Niiyama, D.S. Ahn,
and other Members of the LEPS Collaboration

Beam Time requested: 30 days
Beam Conditions: 2.96 GeV linearly polarized
Detector: standard forward-angle detector
Target: LH_2 15-cm long

Date submitted: 10 September 2006

Summary of Proposal

A recent theoretical paper has shown that the scalar meson of strangeness 1, known as the $\kappa(800)$, contributes to K^* photoproduction through t-channel exchange. A proper description of K^* photoproduction includes s, t and u channel diagrams, but t-channel dominates at forward angles, which is ideally suited to the LEPS spectrometer at SPring-8. Preliminary cross section data from CLAS, at larger angles, suggests that the reaction $\gamma p \to K^{*0}\Sigma^+$ has a significant contribution from κ-exchange (within the theoretical model of Oh and Kim). If so, then the measurement of forward-angle beam spin asymmetries for this reaction, where the theoretical calculations show an unambiguous signal, would establish the role of the $\kappa(800)$. This requires no change to the LEPS detector, but does require a photon beam of between 2.5 and 3.0 GeV, which is now possible at LEPS, although with reduced flux. Count rate calculations suggest that sufficient statistics could be obtained in a 30-day experiment using a 15-cm long liquid hydrogen target.

Using the same beam-time as for the above experiment, a measurement of the recoil polarization in the reaction $\vec{\gamma} p \to K^+\vec{\Lambda}$ is proposed. Using the combination of linearly polarized photons and the parity-violating weak decay $\Lambda \to \pi^- p$, double-polarization observables can be measured. These observables provide detailed information on the production mechanism of $K^+\Lambda$ final state, which will constrain theoretical models of this reaction.

The measurement of both $K^{*0}\Sigma^+$ and $K^+\Lambda$ at once, in the same experiment, provides important restrictions on models of strangeness production processes. Each measurement alone is interesting in its own right, but together they provide a powerful constraint for theoretical calculations.

Detailed Description of the Proposed Research

1. Objectives and Impacts of the K^* Measurement

It is well known in the quark model of hadrons that mesons come in octet (plus a singlet) groups. For the light meson octet, 4 mesons are non-strange and 4 mesons contain either a strange quark or antiquark. The ground state octet consists of pions, kaons and the η-meson. However, the assignments are not so clear for the higher-mass mesons. The Particle Data Group [1], in their note on scalar mesons, states: "In contrast to the vector and tensor mesons, the identification of the scalar mesons is a long-standing puzzle". In particular, the κ-meson with a resonance pole at about 800 MeV is seen in many phenomenological analyses [2] and also in analyses of D-meson decay [3], yet its existence is still contraversial.

The quantum numbers of the I=1/2 κ-meson is $J^P = 0^+$. It is considered to be the positive-parity scalar partner of the kaon in a similar way as the σ-meson partners with the η-meson. The difficulty to establish either the σ or the κ is that their resonance widths are very broad (about 400 MeV or even higher) and hence they are very difficult to see in partial wave analyses of meson scattering data. In the case of D-meson decay [3], there is a need in the decay amplitude for $D^+ \to K^-\pi^+\pi^+$ of an additional $K\pi$ resonance, with the quantum numbers of the κ, which improves the χ^2 for their fit by a factor of 4. However, additional evidence is needed before the κ meson can be established.

In terms of the quark model, the light scalar mesons are difficult to accommodate. The assignments for $J^{PC} = 0^{++}$ are filled by the higher-mass $a_0(1450)$ and $f_0(1370)$ plus $f_0(1710)$ mesons, along with the $K^*(1430)$. In contrast, the light scalar mesons, consisting of the $a_0(980)$ and σ plus $f_0(980)$ along with the κ, are usually considered as meson-meson (or 4-quark) states [4, 5] and are not included in the classical quark model picture [1]. The $a_0(980)$ and $f_0(980)$ are firmly established, but their interpretation as exotic 4-quark states are still in question. More information on the structure of this group of resonance states is desired [6].

As mentioned above, the σ (also called the $f_0(600)$ by the PDG) has a width almost equal to its mass, and certainly cannot be described as a typical Breit-Wigner resonance. The κ is not much better, with a central mass of about 800 MeV and a width of about half the mass. Definitive evidence for the σ and/or κ "mesons" would provide a major step forward in establishing the existence of multi-quark states.

The experiment proposed here, to study the linear polarization observables for K^* photoproduction off the proton, has been shown in theoretical models to be sensitive to κ-meson exchange. One model [7] predicts substantial forward-angle polarization effects in the energy range accessible at the SPring-8/LEPS facility. Hence this measurement will provide new information on the κ meson, and perhaps lead to the establishment of this meson (as a complement to D^+ decay). Of course, theoretical progress is required to establish the κ, and such work would be stimulated by experimental results.

2. Theoretical Predictions of K^* production

In general, K^* photoproduction is different from other vector mesons in that Pomeron exchange is absent in the photoproduction of strange mesons. Hence, the reaction mechanism for K^{*0} photoproduction is different from the case of the neutral non-strange mesons (ρ^0, ω and ϕ) where the t-channel has a strong contribution from Pomeron exchange. At low energies, meson exchange also contributes to the t-channel ρ and ω photoproduction, but Pomeron exchange quickly becomes dominant as the photon energy increases.

For K^{*0} photoproduction, there are few ambiguities in the standard theoretical models at forward angles. A single diagram dominates the t-channel, where a K^0 is exchanged and absorbs the photon through the $M1$ multipolarity, which (in the quark model) flips the spin of one of the quarks. The hadronic coupling of the K^0 to the proton, $g_{KN\Sigma}$, is known from kaon scattering data. Also, the exchange of the K^{*0} is suppressed, since only higher (non-spin-flip) multipolarities can contribute to K^{*0} photoproduction. Furthermore, the contact term (seagull diagram) is proportional to the vector meson change, and disappears for neutral K^* produciton [7].

This results in a simple, controlled calculation for forward-angle K^{*0} photoproduction. However, κ-exchange can also contribute to the t-channel, and so deviations from the standard (no κ-exchange) model would provide clear evidence for the existence of the $\kappa(800)$.

In Ref. [7], both $\gamma p \to K^{*+}\Lambda$ and $\gamma p \to K^{*0}\Sigma^+$ reactions are studied. These reactions proceed by a different mechanism than for kaon photoproduction to the same hyperon final states. In particular, $\kappa(800)$ exchange is prohibitied in kaon photoproduction, but can contribute for K^* photoproduction. As mentioned above, K^* exchange is suppressed in the neutral channel K^{*0} photoproduction, but is allowed in K^{*+} production, and so κ-exchange plays a significant role in the former but only a mild role in the latter [7].

Predictions for the total cross section are shown in Fig. 1 for both K^{*+} and K^{*0} photoproduction and compared with data from Jefferson Lab at $E_\gamma = 3.0$ GeV. The solid line shows the model without κ-exchange, whereas the dashed line includes κ-exchange. As expected, there is a larger contribution of κ-exchange for K^{*0} production, since K^* exchange is absent in this case.

The parity asymmetry [7], given in terms of the spin density matrix elements by $P_\sigma = 2\rho^1_{1-1} - \rho^1_{00}$, is shown in Fig. 2 as a function of the center-of-mass angle θ_{K^*}. Here, there is a large effect of κ exchange in both K^{*+} and K^{*0} production at forward angles. In other words, the parity asymmetry projects out the κ contribution in the t-channel. In this case, scalar κ exchange has positive parity and the pseudoscalar kaon has negative parity.

The parity asymmetry is closely related to the photon beam asymmetry, $\Sigma = (\rho^1_{11} + \rho^1_{1-1})/(\rho^0_{11} + \rho 1 - 1^0)$, and when the helicity is conserved, they are almost equal. This demonstrates the effectiveness of the beam asymmetry to isolate the effects of a particular physics diagram.

The technique to extract the density matrix elements is known, and the details are left to the Appendix (written by T. Mibe, along with notes from Y. Oh). Because the

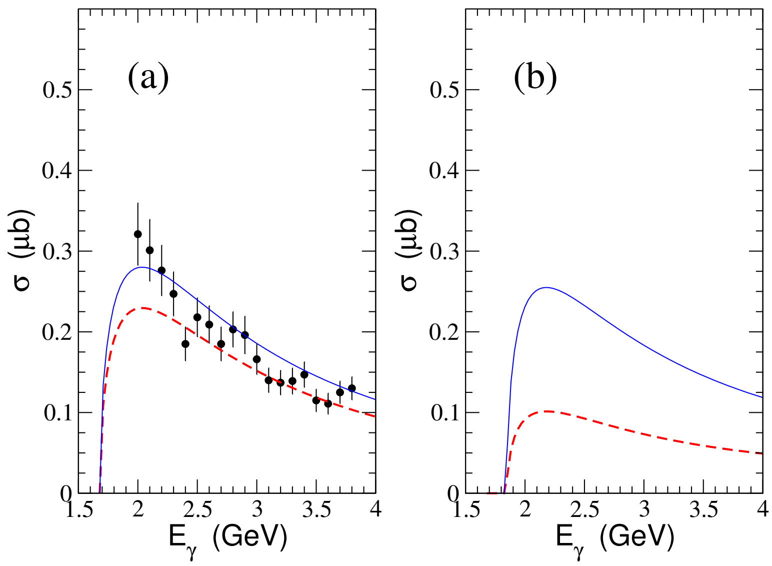

Figure 1: Total cross sections for (a) $\gamma p \to K^{*+}\Lambda$ and for (b) $\gamma p \to K^{*0}\Sigma^{+}$. The dashed (solid) lines are the results without (with) κ-exchange in the model of Oh and Kim [7].

effects shown in Fig. 2 are so large, it should be easy to see the effects of κ exchange using the high linear polarzation of the LEPS beam.

3. Objectives of the $K^+\vec{\Lambda}$ Measurement

An outstanding problem in baryon spectroscopy is the understanding of the missing resonances. For example, the $SU(6) \times O(3)$ symmetry of constituent quark models predict many more resonances than have been thus far observed. One solution is to restrict the number of internal degrees of freedom by assuming that two quarks are bound in a diquark pair, thus lowering the level density of baryon resonances. Another possibility is that some of missing resonances tend to couple weakly to the πN channel, but strongly to non-pionic or strange channels, such as $K\Lambda$ and $K\Sigma$.

Strangeness photoproduction with polarization observables will provide additional information about the baryon resonances and also provide constraints in identifying these resonances, since most of our information on the baryon resonance spectrum comes from the pion-induced or pion-production reactions. When the incoming photons are linearly (circularly) polarized, then this polarization may be transfered in whole or in part to the spin orientation of the produced hyperons within the reaction plane. O_x and O_z (C_x and C_z) characterize the polarization transfer from a linearly (circularly) polarized beam to a recoiling hyperon along orthogonal axes in the reaction plane.

Recent measurements of differential cross sections have been published by groups

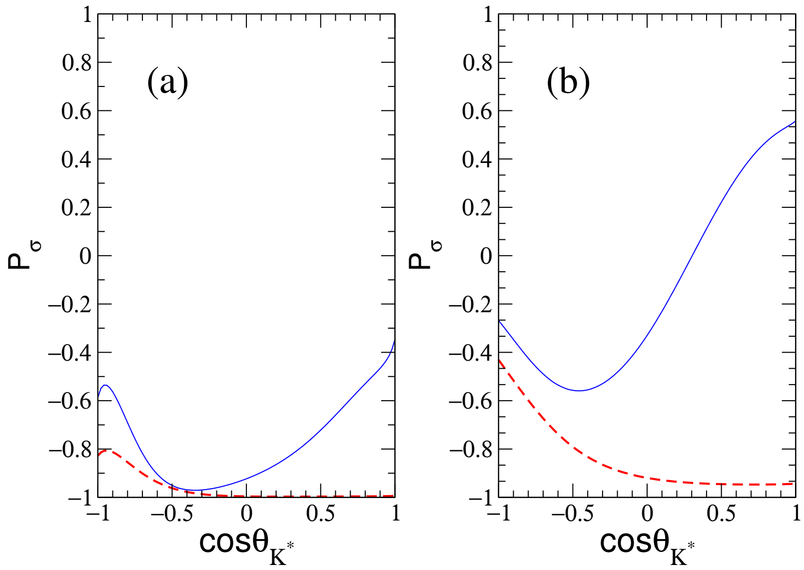

Figure 2: Parity spin asymmetry for (a) $\gamma p \to K^{*+}\Lambda$ and for (b) $\gamma p \to K^{*0}\Sigma^+$ at $E_\gamma = 3.0$ GeV. The dashed (solid) lines are the same as the previous figure.

working at Jefferson Lab [8], Bonn [9], and Spring-8 [10]. Induced hyperon polarizations, P, have also been published by Jefferson Lab [11], Bonn [12], and GRAAL [12]. The linear beam polarization asymmetry, Σ, was measured at SPring-8 [13]. Very sparse data exist on the beam asymmetry, T, from Bonn. There has been presented a preliminary result for recoil polarization observables, O_x and O_z induced by circulary polarized photons at Jefferson Lab [15]. However no published data exist for the hyperon recoil polarization observables O_x and O_z induced by linearly polaried photons. A preliminary analysis for O_x and O_z at Spring-8 using existing data shows limited statistics and limited kinematic coverage [16].

We propose to make high statistical measurements of the recoil polarization observables O_x and O_z of the photoproduction from the proton of two ground state hyperons, namely the reactions $\vec{\gamma} + p \to K^+ + \vec{\Lambda}$ and $\vec{\gamma} + p \to K^+ + \vec{\Sigma}$, where the photon beam is linearly polarized. The data will be obtained using the LEPS detector at Spring-8 for center of mass energies W between 1.9 and 2.5 GeV. These measurements also utilize the newly constructed time-projection-chamber (TPC) to improve kinematic coverage.

4. Recoil Hyperon Polarization Observables

The recoil hyperon polarization observables can be measured by taking advantage of the fact that the Λ and Σ hyperons are self analyzing. When a linearly polarized photon beam and unpolarized proton are used, the three recoil polarization observables can be extracted from the expression of the polarized cross section:

$$\frac{d\sigma}{d\Omega} = \sigma_0\{1 + P_{lin}\Sigma\cos 2\phi + P_x P_{lin} O_x \sin 2\phi + P_y P + P_z P_{lin} O_z \sin 2\phi\} \quad (1)$$

where P_{lin} is the linear photon polarization, and ϕ is the angle between the photon polarization vector and the reaction plane.

The hyperon recoil polarizations are measured through the decay angular distributions. The decay $\Lambda \to \pi^- p$ has a parity-violating weak decay angular distribution in the Λ rest frame. The decay of the Σ proceeds first via an $M1$ radiative decay to a Λ. In either case, the recoil polarization is measured using the angular distribution of the decay protons in the hyperon rest frame. This parity violating weak decay distribution, $I(\cos\theta_i)$, is given by

$$I(\cos\theta_i) = \frac{1}{2}(1 + \alpha P_i \cos\theta_i) \quad (2)$$

where $i = x, y, x$ is one of the three axes in the specified coordinate system and θ_i is the proton polar angle with respect to the given axis in the hyperon rest frame. The weak decay asymmetry, α, is taken to be 0.642.

5. Experimental method and apparatus

This measurement is ideally suited to the forward angles measured by the LEPS detector and the energy of the linearly polarized photon beam available at BL33 at SPring-8. The LEPS detector has been described elsewhere [17] and is unnecessary to repeat here.

The only changes from the standard LEPS setup are:

1. a higher-frequency laser must be used in order to reach up to 3.0 GeV where the calculations predict large effects;

2. the standard aerogel cerenkov counter must be replaced with a gas cerenkov detector having a higher threshold for pions ($p_\pi > 2$ GeV/c will not trigger the cerenkov veto).

The gas cerenkov can be the same as the one used for Sakaguchi's experiment for K^0 detection. A slide from the presentation by Sakaguchi at the 2003 Hypernuclear Conference is shown in Fig. 3. In the present case, the K_S in the figure should be replaced by the K^* and the outgoing π^+ should be replaced with a K^+. As shown in the figure, it is necessary to move the LH2 target further upstream, which will slightly decrease the solid angle of the LEPS spectrometer.

The need for the gas cerenkov is shown by Fig. 4 where the momentum of the π^- from the decay of the K^* is shown for various bins in the CM angle of the K^*. This kinematic plot was generated using 2-body phase space for $K^*\Sigma^+$ events with photon energy between 2.5-3.0 GeV, in the range of lab angles where both K^+ and π^- from K^* decay are detected in the LEPS spectrometer. The momentum of the π^- has the majority of events above 1.0 GeV. The standard aerogel cerenkov counter has minimum index of refraction of n=1.008, which corresponds to a pion momentum threshold of 0.999 GeV. Clearly, the aerogel cerenkov would veto most of the K^* events, whereas the gas cerenkov, with its pion momentum threshold of 2.0 GeV will not veto any K^* events.

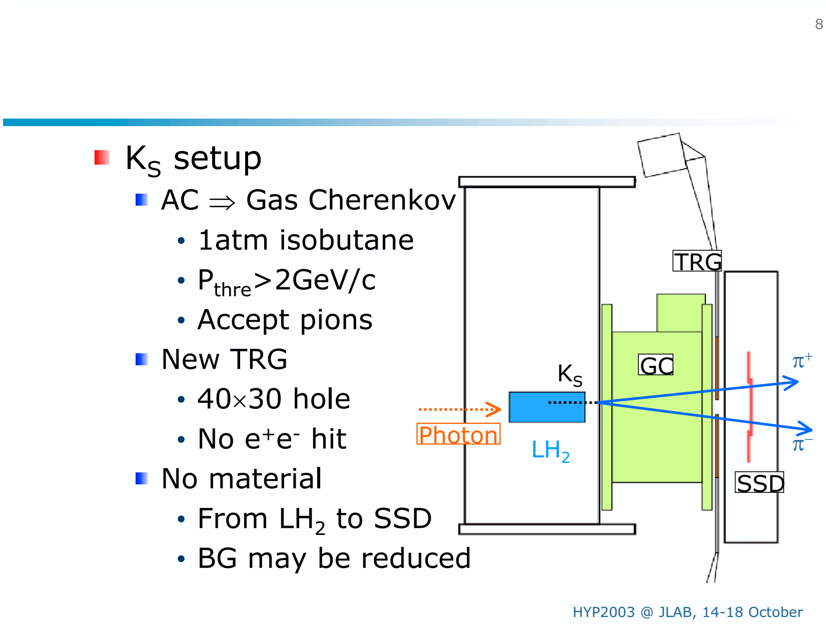

Figure 3: The gas cerenkov detector used in the LEPS experiment for detection of the $\pi^+\pi^-$ pair from K_s^0 decay. This slide is taken from Ref. [18].

The target for this experiment will be the 15-cm long liquid hydrogen (LH2) vessel. Because the cross sections are small (about 50 nb/sr at forward angles), the target length should be as long as possible. The vertex reconstruction for two-particle decays provides good enough resolution to cleanly separate the target from the start counter.

6. Beam Time Request

The photon beam flux with the new laser was measured [19] to be between 7 to 10 kHz per 0.1 GeV bin in the region from 1.5-3.0 GeV. The cross section in the region from 2.5-3.0 GeV is about 60 nb/sr. Taking a cone of polar angle 20°, the solid angle is about 72 sr. Finally, the area number density of hydrogen nuclei for the 15 cm LH2 target is about 6×10^{23} per cm^2. Putting these numbers together, the average count rate is:

$$R = (10^4/sec)(6 \times 10^{23}/cm^2)(60 \times 10^{-30} cm^2/sr)(72 sr)$$

or about 26 counts per second for a perfect detector.

Of course, the detector is not perfect, so the actual count rate will be less. In particular, the efficiency to detect both decay products from the K^{*0} into the LEPS solid angle is small, a few percent, and decreases as the K^* angle increases. Also

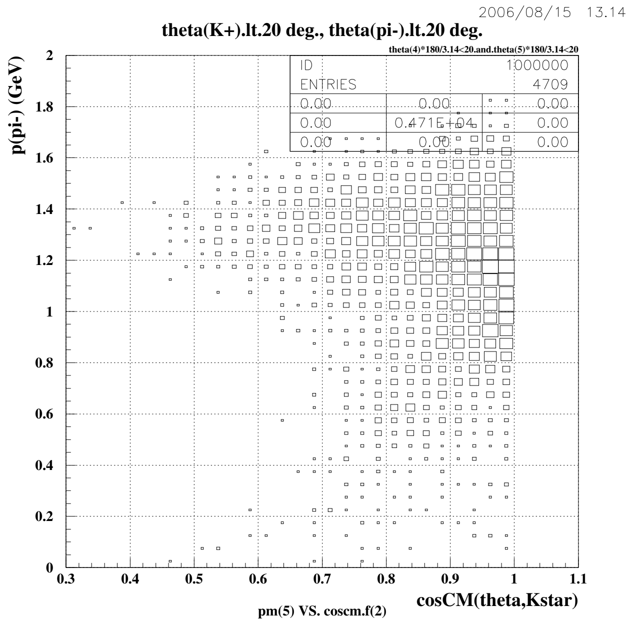

Figure 4: The pion momentum from the decay of the K^* as a function of the cosine of its CM angle. (This plot was provided by T. Mibe using a phase space distribution.)

there is the solid angle obscured by the lead blocker bar and the hole for the pair-produced electrons at 0°. Finally, there is the trigger efficiency and the deadtime of the data acquisition system. Taking these effects into account, we expect about than 0.1 count/second over the entire solid angle, per 0.1 GeV bin of the photon beam (*e.g.*, from 2.8-2.9 GeV).

As shown in the appendix, we need about 10 bins in the azimuthal angle ϕ for each polarization direction (horizontal and vertical). In addition, we want to bin the data in polar angles of 2 degrees. This reduces the count rate per angular bin by a factor of 100.

The background for K^{*0} detection is not known, but based on data from CLAS, we expect a peak-to-background ratio of about one-to-one. In order to fit the peak cleanly, with this signal/noise ratio, we need about 1000 counts in the peak to obtain a statistical precision in the peak fit of about 5%. Hence the total number of counts over all bins is about 10^5 counts for each polarization direction.

For an expected rate of 0.1 counts/sec, about 8500 counts per day can be obtained, or about 12 days to get 10^5 counts for each polarization direction, or 24 days total. There will also be unexpected delays to to unknown trouble, and so we request 30 calendar days of running for the full experiment.

7. Experimental Schedule

It is desirable for the experiment to be scheduled in the summer, when classes are not in session in the USA. This will allow for a long visit by the spokesman during the run. It might also be possible to schedule the experiment to run during the month of December, when there are no classes at Ohio University.

This experiment does not require additional new equipment or any delay for development of detection techniques. The experiment could, in principle, be scheduled at the earliest opportunity.

References

[1] Particle Data Group, Phys. Lett. **B592**, 1 (2004).

[2] D.V. Bugg, Phys. Lett. **B572**, 1 (2003).

[3] E.M. Aitala *et al.*, Phys. Rev. Lett. **89**, 121801 (2002).

[4] R. Jaffe, Phys. Rev. D **15**, 267 (1977).

[5] M. Alford and R.L. Jaffe, Nucl. Phys. **B578**, 367 (2000).

[6] C. Amsler and N. Tornqvist, Phys. Rep. **389**, 61 (2004).

[7] Y. Oh and H. Kim, Phys. Rev. C **74**, 015208 (2006).

[8] R. Bradford, *et al.*, Phys. Rev. C **73**, 035202 (2006).

[9] K.-H. Glander, *et al.*, Eur. Phys. J. **19**, 251 (2004).

[10] M. Sumihama, *et al.*, Phys. Rev. C **73**, 035214 (2006).

[11] J.W.C. McNabb, *et al.*, Phys. Rev. C **69**, 042201 (2004).

[12] A. Lleres, *et al.*, Eur. Phys. J. (to be published) (2006).

[13] R.G.T. Zegers, *et al.*, Phys. Rev. C **91**, 092001 (2003).

[14] K.H. Althoff, *et al.*, Nucl. Phys. **B137**, 269 (1978).

[15] R. Bradford and R.A. Schumacher, to be published in the proceedings of the Nstar 2005 Conference (2006).

[16] M. Sumihama, private conversation.

[17] T. Nakano *et al.*, Nucl. Phys. **A670**, 332 (2000); *ibid*, **A721**, 112 (2003).

[18] A. Sakaguchi, presentation at the HYP2003 Conference.

[19] N. Muramatsu, email sent on 11 August 2006.

August 11, 2006

Note for LEPS proposal on K^* photoproduction

TSUTOMU MIBE
Department of Physics, Ohio University

Abstract

This note describes the technique to extract information on t-channel exchange process via decay angular distributions in vector meson photoproduction with linearly polarized photon beam.

1 Notations and formalism

The decay angular distribution of vector-meson contains rich information on the reaction mechanism. We consider a two-body vector-meson decay (e.g. $K^* \to K\pi, \phi \to K\bar{K}$). The vector-meson rest frame is commonly used in the analysis of the decay angular distributions. There are several ways of defining the quantization axis (z-axis) in the frame. We choose a direction of the incoming photon as a z-axis. This choice of z-axis is so-called the Gottfried Jackson (GJ) frame. The GJ frame is the most suitable frame for analyzing the t-channel exchange mechanisms since some of the t-channel exchange amplitudes have a simple helicity-conserving form which is independent of the momentum transfer [1]. In the GJ frame, production plane is defined as a plane on which momentum vectors of the incoming photon and produced vector-meson lie. Some papers use another choice of z-axis which is equal to a opposite to outgoing proton in the vector meson rest frame (helicity frame). Difference between the GJ frame and the helicity frame is small at very forward vector-meson production angles where the vector mesons go to the direction of the incident photon beam (therefore opposite to outgoing proton). The y-axis is defined as a direction normal to the production plane, the x-axis is defined as a direction of outer product $\hat{y} \times \hat{z}$.

We define the following angles ; ϕ, Φ, and θ. θ is the polar angle between the a decay particle and the vector-meson production plane in the vector-meson rest frame. ϕ is an azimuthal angle between the decay particle and the vector-meson production plane in the vector-meson rest frame. Φ is an azimuthal angle between the photon polarization vector and the vector-meson production plane in the overall center-of-mass frame. For example, the definitions of these angles are shown in Fig.1 for the ϕ-meson decay (decay angles for $K^* \to K^+\pi^-$ are similarly defined by interchanging $K^- \leftrightarrow \pi^-$).

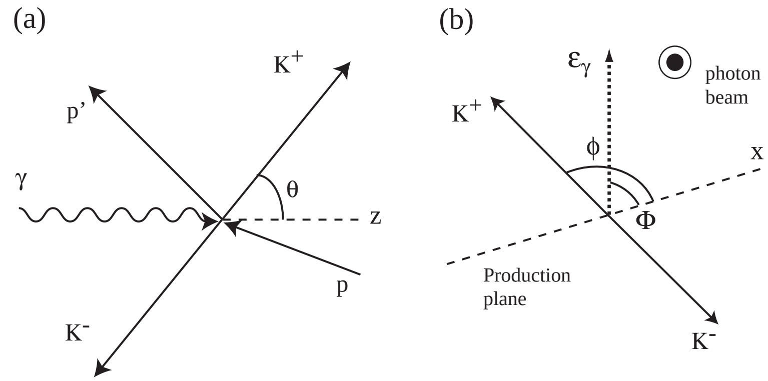

Figure 1: Decay angles (Gottfried-Jackson frame) for the reaction $\gamma + p \to \phi + p \to K^+K^-p$. (a) diagrammatic representation of the system viewed from the x-axis, (b) the system viewed from the z-axis, where the arrow with $p(p\prime)$ stands for direction of the incident (outgoing) proton, and ϵ_γ represents the direction of the photon polarization.

The decay angular distribution $W(\phi,\theta,\Phi)$ for vector-meson photoproduction by linearly-polarized photons are expressed using nine spin-density matrix elements ρ^0,ρ^1,ρ^2 and the polarization degree of the photon beam P_γ [2]:

$$W(\phi,\theta,\Phi) \;=\; (W^0(\phi,\theta) - W^1(\phi,\theta)P_\gamma \cos 2\Phi - W^2(\phi,\theta)P_\gamma \sin 2\Phi) \qquad (1)$$

where, $W^0(\phi,\theta)$ is the polarization-independent part and $W^1(\phi,\theta)$ and $W^2(\phi,\theta)$ are polarization-dependent parts. W^0, W^1 and W^2 are represented in following form:

$$\begin{aligned}
W^0(\phi,\theta) &= \frac{3}{4\pi}(\frac{1}{2}(1-\rho^0_{00}) + (3\rho^0_{00}-1)\cos^2\theta \\
&\quad -\sqrt{2}Re\rho^0_{10}\sin 2\theta\cos\phi - \rho^0_{1-1}\sin^2\theta\cos 2\phi), \\
W^1(\phi,\theta) &= \frac{3}{4\pi}(\rho^1_{11}\sin^2\theta + \rho^1_{00}\cos^2\theta \\
&\quad -\sqrt{2}Re\rho^1_{10}\sin 2\theta\cos\phi - \rho^1_{1-1}\sin^2\theta\cos 2\phi), \\
W^2(\phi,\theta) &= \frac{3}{4\pi}(\sqrt{2}Im\rho^2_{10}\sin 2\theta\sin\phi + Im\rho^2_{1-1}\sin^2\theta\sin 2\phi). \qquad (2)
\end{aligned}$$

The spin-density matrix elements (ρ^I_{jk} with $I = 0,1,2$ and $j,k = -1,0,1$) are bilinear combinations of scattering amplitude. We follow the standard definition given in Ref. [3]:

$$\begin{aligned}
\rho^0_{\lambda\lambda'} &= \frac{1}{N}\sum_{\alpha,\lambda_\gamma} I_{\alpha;\lambda,\lambda_\gamma}\, I^\dagger_{\alpha;\lambda',\lambda_\gamma}, \\
\rho^1_{\lambda\lambda'} &= \frac{1}{N}\sum_{\alpha,\lambda_\gamma} I_{\alpha;\lambda,-\lambda_\gamma}\, I^\dagger_{\alpha;\lambda',\lambda_\gamma}, \\
\rho^2_{\lambda\lambda'} &= \frac{i}{N}\sum_{\alpha,\lambda_\gamma} \lambda_\gamma I_{\alpha;\lambda,-\lambda_\gamma}\, I^\dagger_{\alpha;\lambda',\lambda_\gamma}, \qquad (3)
\end{aligned}$$

where I represents the scattering amplitude, and N is a normalization factor. λ_γ, λ ($\lambda\prime$) are spin projection of the incoming photon, outgoing vector meson, respectively. α is a set of the other quantum numbers including the polarization of the incoming and outgoing proton.

The scattering amplitude I consists of helicity conserving amplitude ($\equiv I_{\lambda,\lambda}$) and helicity non-conserving amplitude ($\equiv I_{\lambda,\lambda'}$ with $\lambda \neq \lambda'$). When only helicity-conserving amplitudes are present in the process, the elements ρ^1_{1-1} and $\mathrm{Im}\rho^2_{1-1}$,which contain products of helicity-conserving amplitudes, are possible to have non-zero values and all the other elements are zero, i.e.

$$
\begin{aligned}
\rho^1_{1-1} &= \frac{1}{N}\sum_{\alpha,\lambda_\gamma} I_{1,-\lambda_\gamma}\, I^\dagger_{-1,\lambda_\gamma} \\
&= \frac{1}{N}\sum_{\alpha} I_{1,-1}\, I^\dagger_{-1,1} + I_{1,1}\, I^\dagger_{-1,-1} \\
&= \frac{1}{N}\sum_{\alpha} I_{1,1}\, I^\dagger_{-1,-1} \\
&= -\mathrm{Im}\rho^2_{1,-1} \\
& \rho^0_{00} = \rho^0_{1-1} = \mathrm{Re}\rho^0_{10} = \rho^1_{00} = \mathrm{Re}\rho^1_{10} = \rho^1_{11} = \rho^2_{10} = 0.
\end{aligned} \tag{4}
$$

Examples of the helicity-conserving amplitude are t-channel scalar exchange, Pomeron exchange (natural-parity exchange) and pseudo-scalar (K, π, η) exchange (unnatural-parity exchange) processes in forward angles. Pure natural-parity exchange gives $\rho^1_{1-1} = -\mathrm{Im}\rho^2_{1-1} = +1/2$, while pure unnatural-parity exchange gives $-1/2$. When both of these two contribute to the scattering amplitude with a relative weight β ($I_{tot} = \sqrt{1-\beta^2} I^N + \beta I^{UN}$), the spin-density matrix elements are given by

$$
\rho^1_{1-1} = -\mathrm{Im}\rho^2_{1-1} = \frac{1-2\beta^2}{2}, \tag{5}
$$

and all the other elements are zero. Therefore, information on ρ^1_{1-1} and $\mathrm{Im}\rho^2_{1-1}$ provides the relative weight (β) between natural-parity exchange and unnatural-parity exchange. Similarly, parity asymmetry (P_σ) and decay asymmetry (Σ_V) are often discussed in the literature. They are defined as

$$
\begin{aligned}
P_\sigma &\equiv \frac{\sigma^N - \sigma^N}{\sigma^N + \sigma^N} \simeq 2\rho^1_{1-1} - \rho^1_{00}, && (6) \\
\Sigma_V &\equiv \frac{\sigma^\parallel - \sigma^\perp}{\sigma^\parallel + \sigma^\perp}, = \frac{1}{P_\gamma}\frac{W(0,\frac{\pi}{2},\frac{\pi}{2}) - W(0,\frac{\pi}{2},0)}{W(0,\frac{\pi}{2},\frac{\pi}{2}) + W(0,\frac{\pi}{2},0)} = \frac{\rho^1_{11}+\rho^1_{1-1}}{\rho^0_{11}+\rho^0_{1-1}}, && (7)
\end{aligned}
$$

where σ^N and σ^U are cross sections for natural and unnatural parity exchanges, and $\sigma_\parallel$ and $\sigma_\perp$ are cross sections at at $\cos\theta = 0, \Phi = 0$ and $\cos\theta = 0, \Phi = \frac{\pi}{2}$. Under the absence of the helicity non-conserving amplitudes, P_σ is equal to Σ_V, and $P_\sigma = \Sigma_V = +(-)1$ for pure natural-parity exchange (unnatural-parity exchange).

In general, the helicity is not conserved in exchange of non-zero spin particle and s-channel/u-channel amplitudes. When the helicity non-conserving amplitude is present, the other seven spin-density matrix elements could have non-zero value. The helicity conservation of the process is experimentally checked by measuring these density matrix elements.

Experimentally, the three-dimensional angular distribution $W(\phi,\theta,\Phi)$ is an measurable quantity. The spin density matrix elements are extracted from fit to the data with nine free parameters (nine density matrix elements). Practically, performing such a fit in three-dimensional space is difficult as it requires sufficient statistics to cover three-dimensional angular space. Note that the measurement of Σ_V needs ϕ distributions in two photon polarization directions ($\Phi = 0, \frac{\pi}{2}$) at $\cos\theta = 0$. This requires good statistics at the particular choice of angles in three-dimensional angle space.

Although there are some limitations to measure full density matrix elements and Σ_V, most of important information on the t-channel exchange mechanism is often obtained from "reduced"-dimensional angular distributions. The three-dimensional angular distribution $W(\phi, \theta, \Phi)$ can be reduced to one-dimensional distribution for a particular angular variable after integrating over the other remaining angles :

$$\begin{aligned} W(\cos\theta) &= \frac{3}{2}(\frac{1}{2}(1-\tilde{\rho}_1)(1-\cos^2\theta) + \tilde{\rho}_1\cos^2\theta) && (8)\\ W(\phi) &= \frac{1}{2\pi}(1 - 2\tilde{\rho}_2\cos 2\phi) && (9)\\ W(\phi-\Phi) &= \frac{1}{2\pi}(1 + 2P_\gamma\tilde{\rho}_3\cos 2(\phi-\Phi)) && (10)\\ W(\phi+\Phi) &= \frac{1}{2\pi}(1 + 2P_\gamma\tilde{\rho}_4\cos 2(\phi+\Phi)) && (11)\\ W(\Phi) &= \frac{1}{2\pi}(1 - P_\gamma\tilde{\rho}_5\cos 2\Phi), && (12) \end{aligned}$$

where

$$\begin{aligned} \tilde{\rho}_1 &= \rho^0_{00}, && (13)\\ \tilde{\rho}_2 &= \rho^0_{1-1}, && (14)\\ \tilde{\rho}_3 &= (\rho^1_{1-1} - \mathrm{Im}\rho^2_{1-1})/2, && (15)\\ \tilde{\rho}_4 &= (\rho^1_{1-1} + \mathrm{Im}\rho^2_{1-1})/2, && (16)\\ \tilde{\rho}_5 &= 2\rho^1_{11} + \rho^1_{00}, && (17) \end{aligned}$$

Experimentally, $\tilde{\rho}_1 - \tilde{\rho}_5$ are obtained from a fit to the one-dimensional distributions from data. The helicity conserving natural-parity (unnatural-parity) exchange processes give $\tilde{\rho}_3 = +(-)\frac{1}{2}$ and $\tilde{\rho}_1 = \tilde{\rho}_2 = \tilde{\rho}_3 = \tilde{\rho}_5 = 0$.

2 Examples

In the previous section, we showed measurement of the decay angular distributions of vector-meson is a powerful tool to decompose the scattering amplitude into a natural-parity exchange part and an unnatural-parity exchange part. We show available experimental data on vector-meson photoproduction to demonstrate how this technique works in experiments.

Figure 2 shows the experimental data for ϕ and ω-meson photoproduction at $E_\gamma = 2.8, 4.7$ and 9.3 GeV [4]. The $\cos\theta$ distributions have revealed a dominance of helicity-conserving amplitude in ϕ and ω-meson photoproduction reactions in these energy ranges, i.e. $\tilde{\rho}_1 \sim 0$. The $\psi(\equiv \phi - \Phi)$ distribution indicates that the natural-parity exchange is favored in the ϕ-meson photoproduction although statistics are poor. On the other hand, there is a clear energy dependence of decay angular distributions for the ω-meson photoproduction. The reduction of modulation in the ψ distribution at lower energies can be understood from increase of π exchange contribution as ω-meson strongly couples to π meson, while π exchange is strongly suppressed in the ϕ-meson photoproduction by the OZI rule.

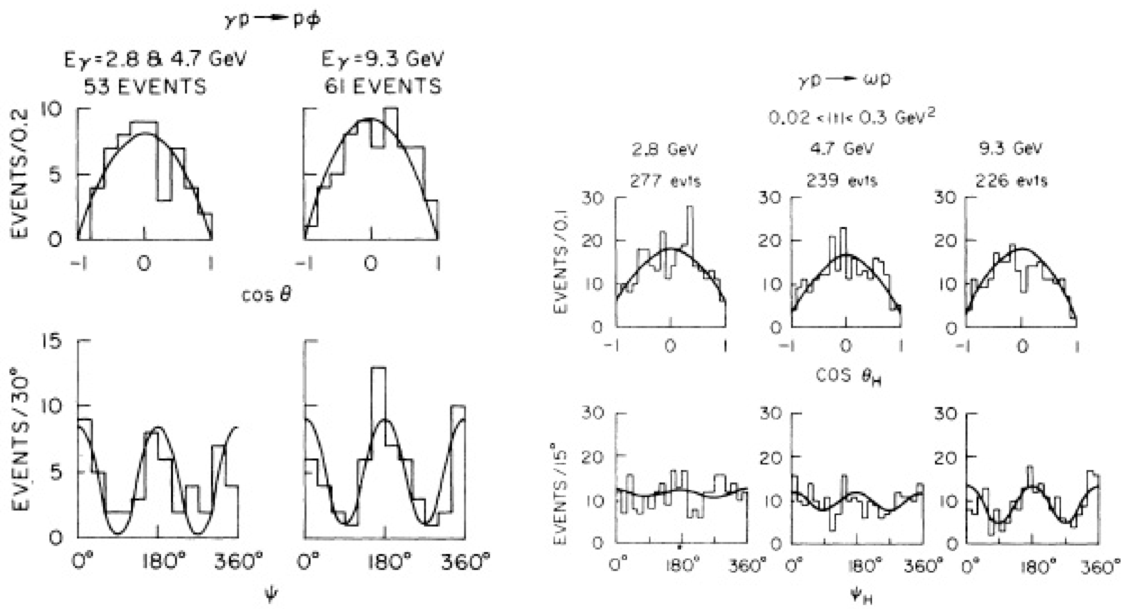

Figure 2: (left) $\cos\theta$ and $\psi(\equiv\ \phi - \Phi)$ distributions for ϕ photoproduction and (right) ω photoproduction [4]. The curves in plots for ϕ photoproduction are the fits to the data assuming helicity conservation in the helicity frame. The curves in plots for ω photoproduction are the fits to the data without assumption of helicity conservation.

Recently, the decay angular distributions in ϕ-meson photoproduction was measured at the LEPS facility with an order of magnitude higher statistics [5]. Figure 3 shows measurements at $-0.2 < t+|t|_{min} \leq 0$ GeV^2 in two energy regions, $1.97 < E_\gamma < 2.17$ and $2.17 < E_\gamma < 2.37$ GeV. The extracted spin-density matrix elements are shown in Table 1. In both energy regions, $W(\cos\theta)$ behaves as $\sim (3/4)\sin^2\theta$, indicating the dominance of helicity-conserving processes (Fig 3(a)). Figure 3(b) shows the distribution $W(\phi-\Phi)$. The positive value for $\tilde{\rho}_3$ indicates that the contributions from natural parity exchange are bigger than those for unnatural parity exchange (π, η-meson exchange). Data also indicates that contribution from unnatural parity exchange is not negligible in low energies (see Fig. 2 for results at higher energy). This is likely due to non-$s\bar{s}$ component of ϕ-meson wave function and/or violation of the OZI rule. The one dimensional angular distributions $W(\phi)$, $W(\phi+\Phi)$ and $W(\Phi)$ are depicted in Fig. 3(c). No strong oscillation was found, except that the distribution $W(\phi)$. These results for the ϕ-meson photoproduction proves the feasibility of measurements of decay angular distribution of vector mesons at the LEPS facility. Similar technique can be employed for measurement of the K^* decay angular distributions.

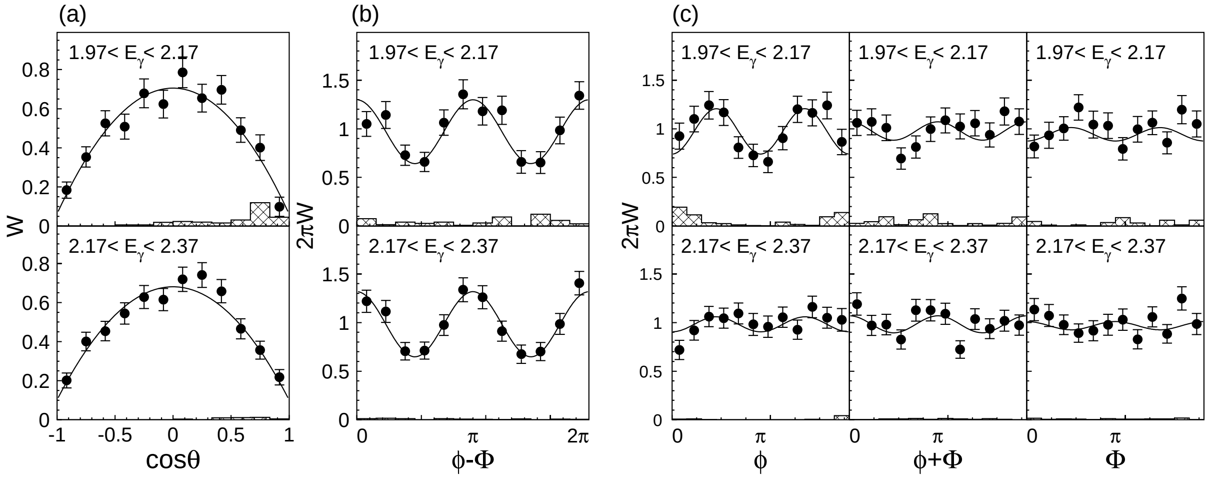

Figure 3: Decay angular distributions for ϕ-meson photoproduction. The solid curves are the fit to the data. The hatched histograms are systematic errors. Data from Ref [5]

Table 1: Spin density matrix elements in ϕ-meson photoproduction (data are from [5].)

Spin density matrix	2.17< E_γ <2.37 GeV (sys. error)	1.97< E_γ <2.17 GeV (sys. error)
$\tilde{\rho_1}$	0.069 ± 0.020 (0.002)	0.042 ± 0.024 (0.008)
$\tilde{\rho_2}$	0.039 ± 0.022 (0.014)	0.120 ± 0.027 (0.011)
$\tilde{\rho_3}$	0.189 ± 0.024 (0.006)	0.197 ± 0.030 (0.022)
$\tilde{\rho_4}$	0.049 ± 0.025 (0.006)	0.056 ± 0.031 (0.012)
$\tilde{\rho_5}$	-0.049 ± 0.048 (0.005)	0.085 ± 0.062 (0.048)

References

[1] A. I. Titov, T. S. H. Lee, H. Toki, and O. Streltsova, Phys. Rev. **C60**, 035205 (1999).

[2] K. Schilling, P. Seyboth, and G. E. Wolf, Nucl. Phys. **B15**, 397 (1970).

[3] A. I. Titov and T. S. H. Lee, Phys. Rev. **C67**, 065205 (2003), `nucl-th/0305002`.

[4] J. Ballam et al., Phys. Rev. **D7**, 3150 (1973).

[5] T. Mibe et al. (LEPS), Phys. Rev. Lett. **95**, 182001 (2005), `nucl-ex/0506015`.